Anisotropic Material Transport by Eddies and Eddy-Driven Currents in a Model of the North Atlantic

IGOR KAMENKOVICH

Rosenstiel School of Marine and Atmospheric Science, University of Miami, Miami, Florida

PAVEL BERLOFF

Department of Mathematics, and Grantham Institute for Climate Change, Imperial College London, London, United Kingdom, and Woods Hole Oceanographic Institution, Woods Hole, Massachusetts

JOSEPH PEDLOSKY

Woods Hole Oceanographic Institution, Woods Hole, Massachusetts

(Manuscript received 11 February 2009, in final form 25 June 2009)

ABSTRACT

This study analyzes anisotropic properties of the material transport by eddies and eddy-driven zonal jets in a general circulation model of the North Atlantic through the analysis of Lagrangian particle trajectories. Spreading rates—defined here as half the rate of change in the particle dispersion—in the zonal direction systematically exceed the meridional rates by an order of magnitude. Area-averaged values for the upper-ocean zonal and meridional spreading rates are approximately 8100 and 1400 $m^2\ s^{-1}$, respectively, and in the deep ocean they are 2400 and 200 $m^2\ s^{-1}$. The results demonstrate that this anisotropy is mainly due to the action of the transient eddies and not to the shear dispersion associated with the time-mean jets. This property is consistent with the fact that eddies in this study have zonally elongated shapes. With the exception of the upper-ocean subpolar gyre, eddies also cause the superdiffusive zonal spreading, significant variations in the spreading rate in the vertical and meridional directions, and the difference between the westward and eastward spreading.

1. Introduction

Mesoscale eddies represent one of the main vehicles for tracer transport in the oceans. Predominantly along-isopycnal eddy fluxes of temperature and salinity play an important role in supporting the stratification in the midlatitudes (Radko and Marshall 2004; Henning and Vallis 2005; Cessi and Fantini 2004). Eddy transports of bio- or geochemical tracers affect uptake and distribution of transient atmospheric gases, such as the chlorofluorocarbons (Booth and Kamenkovich 2008) and carbon dioxide. Understanding the eddy dynamics and the adequate representation of eddy transports is thus crucial for accurate prediction of climate change. Since climate models cannot resolve oceanic mesoscale, the eddy effects have to be parameterized by mixing schemes, such as downgradient diffusion. In most parameterization schemes, the diffusivity coefficients are often determined empirically and assumed to be constant. Existing evidence based on direct observations and numerical simulations, however, suggests strongly nonuniform spatial distribution of the eddy effects. The spatial structure of the mesoscale eddies tends to be highly anisotropic (e.g., Huang et al. 2007; Scott et al. 2008; Berloff et al. 2009). The estimates of the diffusivity based on the Lagrangian statistics from drifters suggest that, in the tropical Pacific, the zonal diffusivity is approximately 7 times larger than the meridional one (Bauer et al. 2002) and in the Southern Ocean it is also larger than the meridional diffusivity (Sallee et al. 2008). The diffusivities estimated from float (LaCasce and Bower 2000; Lumpkin et al. 2002) and satellite (Marshall et al. 2006) data also vary strongly with geographical location. Eddy-resolving simulations also demonstrate highly nonuniform spatial distribution of

Corresponding author address: Igor Kamenkovich, 4600 Rickenbacker Causeway, University of Miami, Miami, FL 33149.
E-mail: ikamenkovich@rsmas.miami.edu

DOI: 10.1175/2009JPO4239.1

eddy mixing of temperature and salinity (Gille and Davis 1999; Nakamura and Chao 2000; Roberts and Marshall 2000) and highly anisotropic dispersion (Berloff et al. 2002; Veneziani et al. 2005). Nonuniform spatial distribution of the eddy mixing has important effects on distribution of tracers in eddy-resolving North Atlantic simulations (Booth and Kamenkovich 2008).

One of the important examples of the processes that can influence tracer spreading in the oceans is the phenomenon of the multiple alternating zonal jets. These jets have been detected in altimeter data (Maximenko et al. 2005; Huang et al. 2007), float measurements (Hogg and Owens 1999; Treguier et al. 2003), and eddy-resolving GCMs (Galperin et al. 2004; Nakano and Hasumi 2005; Richards et al. 2006; Kamenkovich et al. 2009, hereafter KBP09). These jets are eddy driven (e.g., Rhines 1994; Thompson and Young 2007; Berloff et al. 2009; KBP09) and are not reproduced by non-eddy-permitting numerical simulations. The presence of the jets can result in the difference between the tracer transports in zonal and meridional directions due to shear dispersion (Taylor 1953; Young et al. 1982). Smith (2005)'s study, with an isotropic eddy field superimposed onto zonally uniform barotropic jets, demonstrates that the shear dispersion in this case results in highly anisotropic mixing. In particular, he demonstrates that the turbulent tracer transport in the direction of the uniform barotropic jets corresponds to diffusivity inversely proportional to the cross-jet diffusivity. The along-jet diffusivity is typically two orders of magnitude greater than the cross-jet diffusivity. One of the objectives of this study is to estimate the significance of shear dispersion in a more complex situation with anisotropic eddies and two-dimensional time-mean flow. Zonally elongated transient eddies, which have a long correlation scale in the zonal direction and are strongly zonally sheared, are expected to lead to a predominantly zonal material transport (see the appendix). To distinguish these effects from those of the time-mean currents in this study, we use the term ''shear dispersion'' as the particle dispersion resulting from the presence of time-mean currents.

The main goal of this study is to characterize the following three aspects of the anisotropic material transports: 1) the difference between the zonal and meridional directions, 2) the nonuniform distributions of transports in the meridional and vertical directions, and 3) the east–west and north–south asymmetry of tracer spreading. Our GCM study is based on Lagrangian particle statistics (e.g., Owens 1984; Davis 1991; also see a review in LaCasce 2008). From the practical point of view, the diffusivities estimated from eddy-permitting simulations can guide the development of the parameterizations of unresolved eddy transports in non-eddy-permitting models. Such parameterizations have to account for the tracer dispersion by the eddies (direct eddy effects) and the spreading of the tracers by eddy-driven flows (indirect eddy effects). The relative importance of the direct and indirect eddy effects on the tracer dispersion is one of the main topics of this study. We address this issue by analyzing spatial structure of the spreading of the Lagrangian particles and by comparing particle trajectories in the flow with and without time-mean eddy-driven currents.

2. Numerical model

The eddy-resolving numerical model of the North Atlantic used in this study is the one used in KBP09, and is only briefly described in this paper. The model is based on the Geophysical Dynamics Laboratory Modular Ocean Model (GFDL MOM) 3.0 code (Pacanowski and Griffies 1999), which solves the equations of motion on fixed geopotential surfaces. The horizontal resolution is $\frac{1}{8}°$ in both latitudinal and longitudinal directions, which permits simulation of mesoscale eddies. Idealized features of the model simplify the spinup and the analysis of results. The domain spans from 14° to 60°N and from 70° to 10°W and conventional sponge boundaries are used at the southern and northern boundaries of the domain. The depth of the ocean is limited to 3000 m, which roughly corresponds to the depth of the North Atlantic Deep Water cell in the real ocean (Talley 2003) and there are 30 vertical levels with thicknesses increasing away from the surface. Model topography is derived from the $1° \times 1°$ Scripps dataset.

The boundary conditions at the free surface and the lateral sponge layers have a form of restoring to the annual-mean values of the temperature and salinity derived from the high-resolution ($\frac{1}{4}°$) analyses of the world's oceans (Boyer et al. 2005). The restoring time scales for temperature and salinity are 60 and 180 days (for a 50-m mixed layer), respectively. The annual-mean zonal and meridional components of the surface wind stress are derived from the National Centers for Environmental Prediction (NCEP) 1979–2001 reanalysis.

Most of the horizontal mixing of momentum, temperature, and salinity is done by the explicitly simulated mesoscale eddies. Small horizontal biharmonic viscosity and diffusion is retained in the model in order to represent submesoscale mixing processes; the coefficients are 10^{11} m^4 s^{-1} and 10^{10} m^4 s^{-1}, respectively. Vertical diffusion is kept at a realistic low value for the ocean above rough topography of 10^{-5} m^2 s^{-1} (Ledwell et al. 1993).

Alternating multiple zonal jets are clearly seen in the time-averaged zonal velocities at all depths. Below approximately 200 m they dominate the time-mean zonal

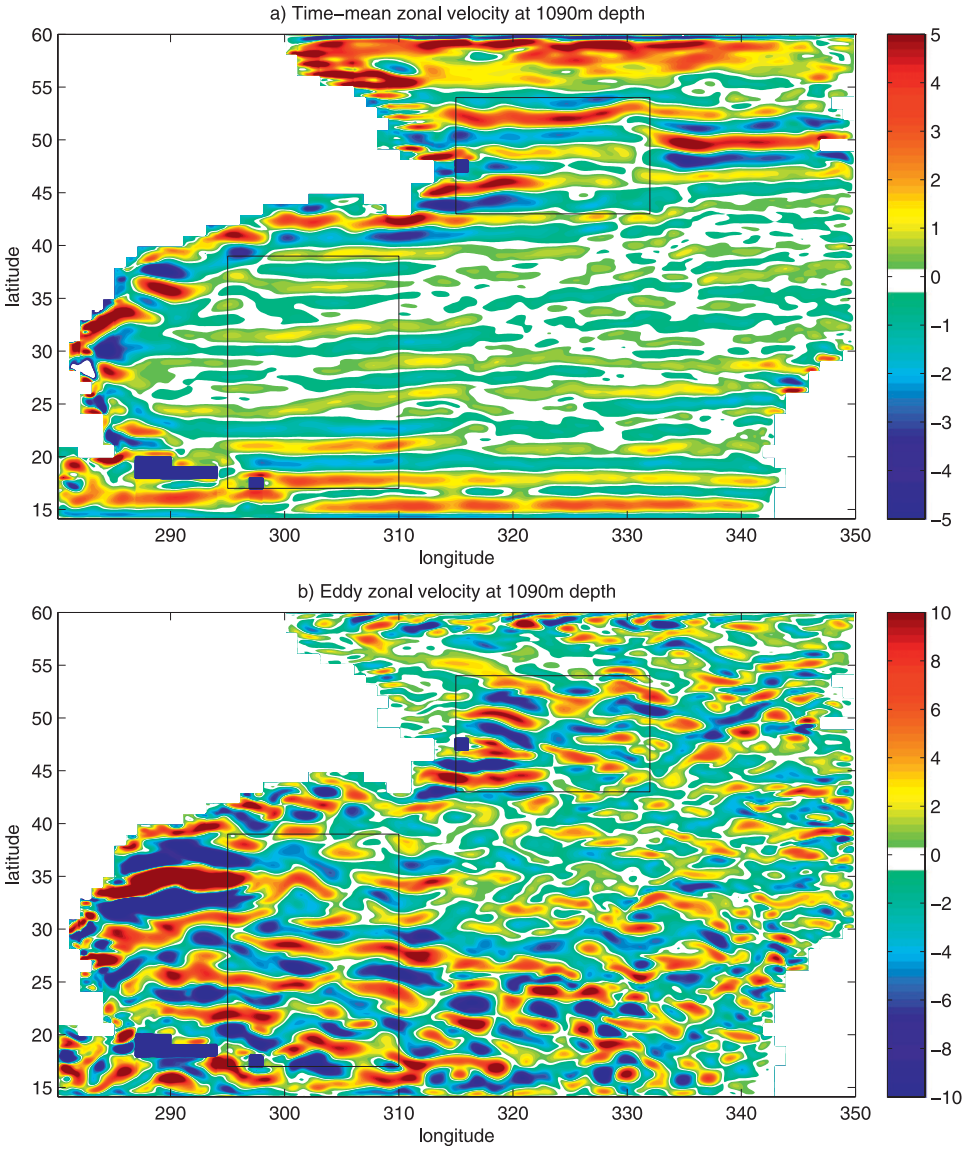

FIG. 1. Time-mean multiple zonal jets and transient eddies in the model. The zonal velocities are at a depth of 1090 m for (a) values averaged over 9 years and (b) instantaneous values with the subtracted time-mean. The units are 10^{-2} m s^{-1}. Two black rectangles mark the regions where the 90 000 neutrally buoyant particles were released in 12 consecutive experiments.

flow (Fig. 1a). In the subpolar gyre, the jets are both strong and nearly steady, whereas in the subtropical gyre they change their position with time, resulting in their weaker time means (KBP09). The jets are "latent," because strong mesoscale variability tends to mask them in the entire domain (Fig. 1b). Because of this latency, it is unclear to what extent the material transport properties are dominated by the jets and this is one of the main questions we raise. The regions of zonal acceleration and deceleration of the jets correspond to significant time-mean meridional velocities (not shown). The jets can, therefore, affect Lagrangian particle spreading through the two-dimensional shear dispersion. As in KBP09, our analysis is concentrated on the western part of the basin, where the jets are most pronounced. Note also the apparent anisotropy of the transient eddies; eddies tend to increase in strength westward, particularly in the subpolar and northern subtropical gyres, and tend to be zonally elongated (Fig. 1b).

3. Spreading of neutrally buoyant particles

Neutrally buoyant Lagrangian particles are released in 12 consecutive 180-day model runs. Each simulation

starts with 90 000 floats that are uniformly distributed between 22 and 2900 m and within two horizontal ''box'' regions (Fig. 1) in the subtropical and subpolar gyres. Solid meridional boundaries and western boundary currents can, respectively, inhibit zonal and enhance meridional motions of the particles. To estimate the sensitivity of the results to the particle positions, we split the full ensemble of particles into two equal subgroups. These are based on the particle initial longitudes of the westernmost and easternmost groups. Our analysis shows that during the 180 days of each run the easternmost half of the particles do not reach the solid boundaries everywhere, except in the upper layers of the subpolar gyre, where strong eastward currents carry the particles toward the solid eastern boundary. In the latter region, the westernmost subgroup remains away from the solid boundaries at all times. Note that the boundary effects will inevitably become important if the experiments were continued for a longer period of time. To make sure that the boundary effects do not change the conclusions, we carry our analysis for the westernmost particles in the upper subpolar gyre and for the easternmost particles in the rest of the domain. We report the difference in results for the westernmost and easternmost subgroups wherever appropriate; however, these differences do not affect the conclusions.

In our Lagrangian analysis, the particle advection is corrected for the ''gyre advection,'' which is defined as the time-mean velocities smoothed with the sliding mean 5° × 5° spatial filter. This correction is done by subtracting a portion of particle displacement that is due to the gyre advection only. Thus, the analysis focuses on the particle displacements due to the joint effect of the transient circulations (such as geostrophic eddies) and concentrated time-mean currents (such as zonal jets). In addition to the standard runs described above, we also performed 12 ''eddy-only'' simulations in which the particles are advected by the zonal and meridional velocities with the removed time-mean component. This effectively eliminates the influence of the shear dispersion associated with the zonal jets and isolates the effects of the transient eddies.

The zonal and meridional dispersions for a group of N particles are defined as

$$D_x(t; y) = \frac{1}{N}\sum_{n=1}^{N}[x_n(t) - X(t)]^2,$$

$$D_y(t; y) = \frac{1}{N}\sum_{n=1}^{N}[y_n(t) - Y(t)]^2, \quad (1)$$

where x_n and y_n are the zonal and meridional ''corrected'' displacements of an nth particle from its initial position; X and Y are the ensemble-mean displacements shown here:

$$X(t) = \frac{1}{N}\sum_{n=1}^{N}x_n(t), \quad Y(t) = \frac{1}{N}\sum_{n=1}^{N}y_n(t)\cdot$$

The rate at which D_x and D_y increase with time is then used to define the zonal and meridional spreading rates:

$$K_x(t) = \frac{1}{2}\frac{\partial D_x}{\partial t}, \quad K_y(t) = \frac{1}{2}\frac{\partial D_y}{\partial t}. \quad (2)$$

The asymptotic behavior of (2) at long times is traditionally used to characterize different dispersion regimes (e.g., LaCasce 2008). In particular, the diffusive regime corresponds to the linear increase of the dispersion with time and (2) provides an estimate for the zonal and meridional diffusivities, assuming that the diffusivity tensor is diagonal along x and y.

In the following analysis we will use the difference between the zonal and meridional spreading rates to describe the anisotropy of the material transport by the flow. Additionally, we will analyze changes in the spreading rates with time, distribution of the spreading rates in the meridional and vertical directions, and the east–west (north–south) asymmetry in the zonal (meridional) material transport.

a. Zonal and meridional spreading rates: Time dependence

We first describe the changes in the zonal and meridional spreading rates with time, over a period of 180 days. Initially rapid changes of both K_x and K_y slow down considerably after approximately day 50 (see Fig. 2). The spreading rate in the zonal direction K_x, however, continues to increase at later times and thus exhibits ''superdiffusive'' behavior. We compute K_x values separately in the upper ocean (upper 360 m, Fig. 2a), in the deep ocean (1444–2095 m, Fig. 2c), and in the subtropical and subpolar gyres. In the subtropical gyre, the values of K_x increase with time from 4000 to almost 10 000 $m^2\ s^{-1}$ in the upper ocean and from 1500 to 3000 $m^2\ s^{-1}$ in the deep ocean. In the subpolar region, the values of K_x are smaller than in the subtropical region; they vary in the range of 5500–7000 $m^2\ s^{-1}$ in the upper and 1700–1900 $m^2\ s^{-1}$ in the deep ocean. These values are in general agreement with the eddy diffusivity estimates in Lumpkin et al. (2002), who also report the largest values in the subtropical gyre of approximately 2000–20 000 $m^2\ s^{-1}$ in the upper and 1000–2000 $m^2\ s^{-1}$ in the deep layers and their estimates in the upper subpolar gyre are roughly 5000–10 000 $m^2\ s^{-1}$. The maximum values in their study were found in the Gulf Stream

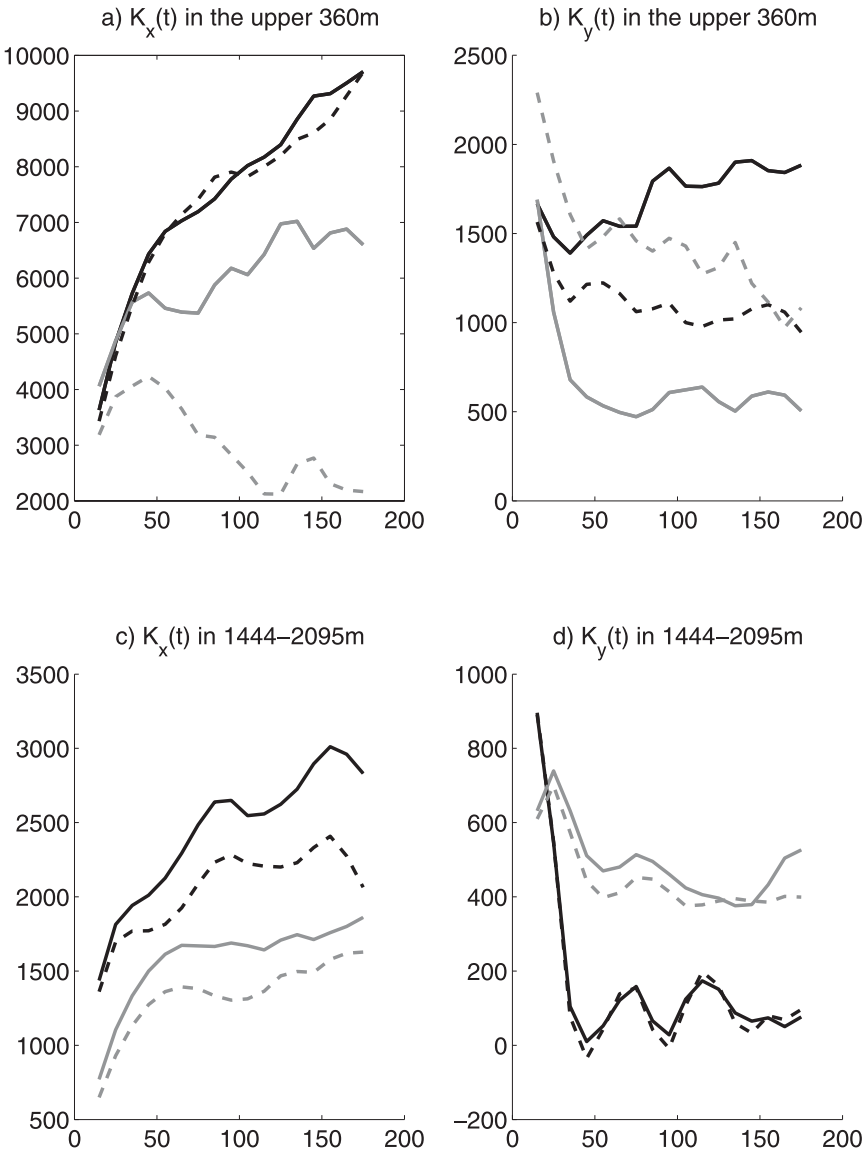

FIG. 2. Particle spreading rate in the zonal and meridional directions, as functions of time. Results from the standard simulations are shown by the solid lines, results from the eddy-only simulations by the dashed lines. The values for the subtropical gyre are shown by the black lines and values for the subpolar gyre by the gray lines. (top) The spreading rate in the upper 360 m in the (a) zonal (K_x) and (b) meridional (K_y) directions. (bottom) The spreading rate in 1444–2095-m depth range in (c) the zonal (K_x) and (d) meridional (K_y) directions. Units are $m^2\ s^{-1}$.

extension area, which is excluded from this analysis because of very strong advective effects. The results between the easternmost and westernmost subgroups in the deep ocean are qualitatively similar but differ in the upper ocean as a result of the boundary effects. In particular, the values of K_x for the easternmost group in the upper-ocean subpolar gyre decrease with time.

The meridional spreading is significantly slower than the zonal one, and K_y also increases with time at a significantly slower rate. In the upper subtropical gyre, the spreading in the meridional direction is superdiffusive, with the values increasing between 1500 and 1900 $m^2\ s^{-1}$. In the deep subpolar gyre and everywhere in the subtropical gyre, the spreading rate fluctuates around a local constant value and does not exhibit a significant trend. In the deep subtropical gyre, K_y values are significantly smaller than in the upper ocean and fluctuate at approximately 100 $m^2\ s^{-1}$; the values in the upper and deep

subpolar gyre fluctuate around 450–550 $m^2 s^{-1}$. The meridional spreading rates are qualitatively similar between the easternmost and westernmost subgroups. However, the easternmost group in the upper-ocean subpolar region and the westernmost subgroup elsewhere exhibit slightly larger spreading rates than those in Fig. 2.

The action by transient eddies is the main cause of the superdiffusive zonal spreading in the subtropical and deep subpolar gyres. In the eddy-only simulations in these regions, the values of K_x (dashed lines) still increase with time. Only the upper-ocean subpolar gyre (Fig. 2a) exhibits nearly diffusive dispersion in the absence of the time-mean currents. The zonal spreading is also noticeably reduced from the standard runs because the reduction is particularly significant (a factor of 3) in the upper subpolar gyre. In contrast, the values of K_y in the upper subtropical gyre are nearly constant in the eddy-only simulations. Another noticeable effect is the sharp increase in the meridional spreading rate in the upper subpolar gyre caused by the removal of the time-mean advection (Fig. 2b). The effects of the time-mean advection on the meridional dispersion in the deep ocean are nearly negligible (Fig. 2d).

b. *Zonal and meridional spreading rates: Spatial distribution*

In this section, we describe the nonuniform distribution of the zonal and meridional spreading rates in the vertical and meridional directions. For the analysis, we discuss the time averages of K_x and K_y between days 100 and 180. The resulting mean spreading rates, denoted by k_x and k_y, would be equivalent to diffusivities if the spreading were purely diffusive. We first calculate $k_x(z)$ and $k_y(z)$ for all particles that are initially located within 100 m of a given depth. Vertical displacements for the vast majority (93%) of the particles are less than 100 m. To account for this nonlocality,[1] the spreading rates are smoothed by a 200-m sliding mean filter.

The largest spreading rates are found in the subtropical gyre (Figs. 3a,c), approximately 10 500 $m^2 s^{-1}$ for k_x and 2800 $m^2 s^{-1}$ for k_y at the surface and k_x = 2750–2850 $m^2 s^{-1}$ and k_y = 140–180 $m^2 s^{-1}$ below 1000 m. The spreading also becomes less isotropic with depth. The measure of spatial anisotropy, defined here as a ratio between zonal and meridional diffusivities, is 3.75 at the surface and reaches a maximum of 22.4 at 750-m depth (Fig. 4a). In the subpolar gyre, the downward decrease in the spreading rates is similarly sharp from the surface values of k_x = 7000 $m^2 s^{-1}$ and k_y = 980 $m^2 s^{-1}$ to the deep values of k_x = 1500–2500 $m^2 s^{-1}$ and k_y = 440–525 $m^2 s^{-1}$. In contrast to the subtropical gyre, the spreading becomes more isotropic with depth and the measure of spatial anisotropy in this region decreases from 7.0 at the surface to less than 3.0 near the bottom (Fig. 4c).

The effect of the time-mean currents on the particle dispersion is modest everywhere, with a noticeable exception in the upper-ocean subpolar gyre. In the eddy-only simulations, both zonal and meridional spreading rates are reduced and the spreading also becomes more isotropic (Figs. 4a,c). The removal of the jet advection causes the depth-averaged measure of anisotropy to decrease from 16.2 to 14.4 in the subtropical gyre region and from 4.9 to 3.0 in the subpolar gyre region. These results signify a modest role of the two-dimensional shear flows in causing anisotropy in the particle spreading.

In the upper-ocean subpolar gyre, the situation is drastically different. In this region, the meridional spreading rate increases sharply (by 50% at the surface) and the zonal spreading rate decreases when the time-mean advection is removed. This result suggests that the effects of the time-mean advection are consistent with those of the one-dimensional, meridionally sheared flow. The corresponding shear dispersion would enhance the zonal and reduce the meridional diffusivities (Smith 2005) and the removal of the time-mean advection would result in more isotropic spreading. Note that although the spreading in the upper-ocean subpolar gyre becomes more isotropic in the eddy-only simulations, the zonal spreading remains more than twice as large as the meridional one (Fig. 4c).

Both the zonal and meridional spreading rates reach their maximum values near the surface and decrease with depth (Figs. 3a–d; see also Lumpkin et al. 2002). The downward decrease in the horizontal eddy velocity magnitude $(u^2 + v^2)^{1/2}$ (Fig. 5) is generally consistent with the downward decrease in the spreading rates. The mean spreading rate $k_H = (k_x^2 + k_y^2)^{1/2}$ from the eddy-only simulations, nevertheless, decreases less rapidly with depth in the subtropical gyre than the eddy velocity magnitude. The velocity magnitude also cannot explain the difference in the spreading rates between the subtropical and subpolar gyres. In particular, the eddy velocities in the upper 250 m of the subtropical gyre are weaker than in the subtropical gyre, whereas k_H in the subtropical gyre is always greater than in the subpolar region.

Can the strong anisotropy of mixing be explained by the presence of zonally elongated eddies? As will be demonstrated in the appendix, transient eddies with the large aspect ratio (the ratio of the zonal to meridional scale) correspond to predominantly zonal time-mean Lagrangian velocities. The eddies in Fig. 1b are indeed

[1] The diffusivities are never strictly local, because of substantial particle displacements; rather, they can be interpreted as average diffusivities within the volume populated by the corresponding particles.

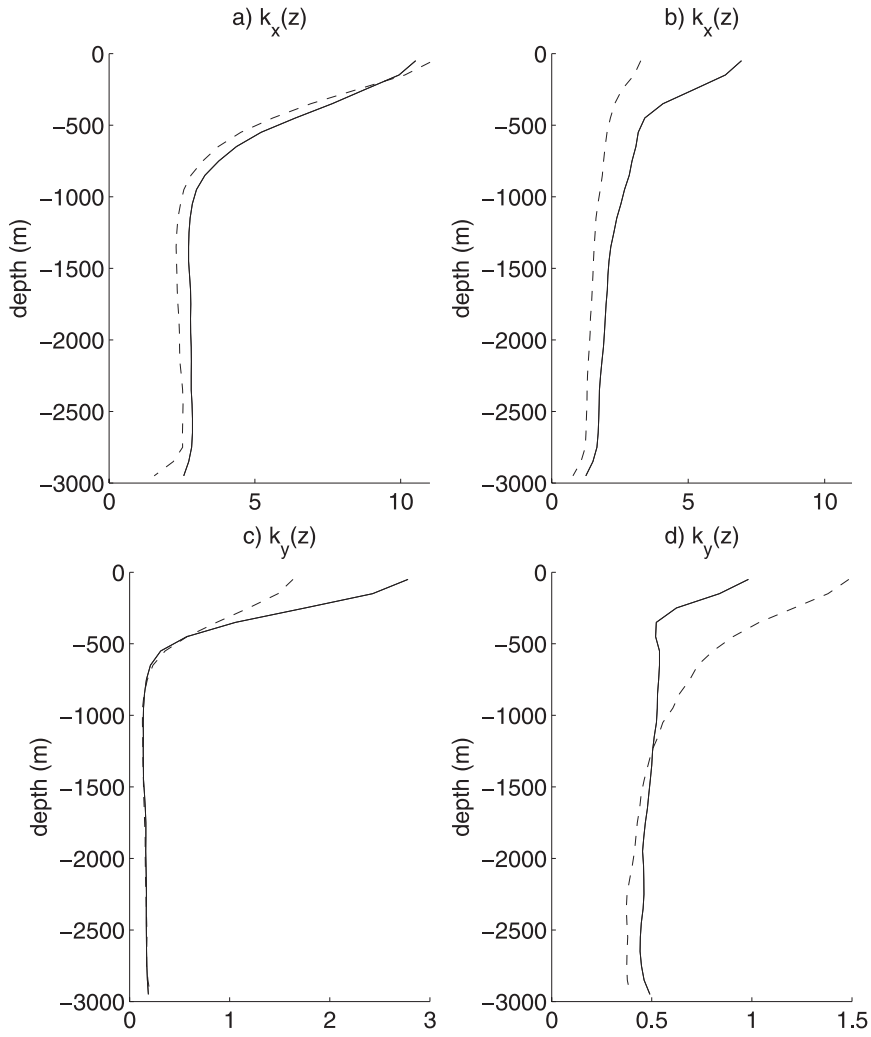

FIG. 3. (a),(b) Zonal (k_x) and (c),(d) meridional (k_y) mean spreading rates as functions of depth. Thin solid lines show the values for the standard simulations, and dashed lines for the eddy-only simulations. Units are $m^2\ s^{-1}$. The results for the entire group of particles are shown for convenience, because the results are qualitatively similar for the easternmost and westernmost subgroups. Note the difference in scale between panels.

visibly stretched in the zonal direction. To further explore this property of eddies, we calculate the time-mean discrete energy spectral densities for zonal and meridional eddy velocities within the subtropical and subpolar box regions in Fig. 1. To quantify the importance of zonally elongated eddies, we define them as modes with an aspect ratio larger than 3/2. We also define meridionally elongated eddies as modes with the aspect ratio smaller than 2/3, and ''round'' eddies as those with an aspect ratio greater than 2/3 but less than 3/2. We then sum energy spectral densities $P_{k,l}$ within each group and for both zonal and meridional velocities and normalize the results by the total energy. The results (Figs. 4b,d) provide an estimate of the portion of the total eddy kinetic energy (EKE) corresponding to each of the three classes of eddies:

$$P_{\text{zon}} = \frac{\sum_{l/k>3/2} P_{k,l}}{\sum_{k,l} P_{k,l}} \quad P_{\text{mer}} = \frac{\sum_{l/k<2/3} P_{k,l}}{\sum_{k,l} P_{k,l}}$$

$$P_{\text{round}} = \frac{\sum_{2/3<l/k<3/2} P_{k,l}}{\sum_{k,l} P_{k,l}}. \tag{3}$$

The spectrum is dominated by zonally elongated eddies, with P_{zon} being between 0.46 and 0.5 in the subtropical

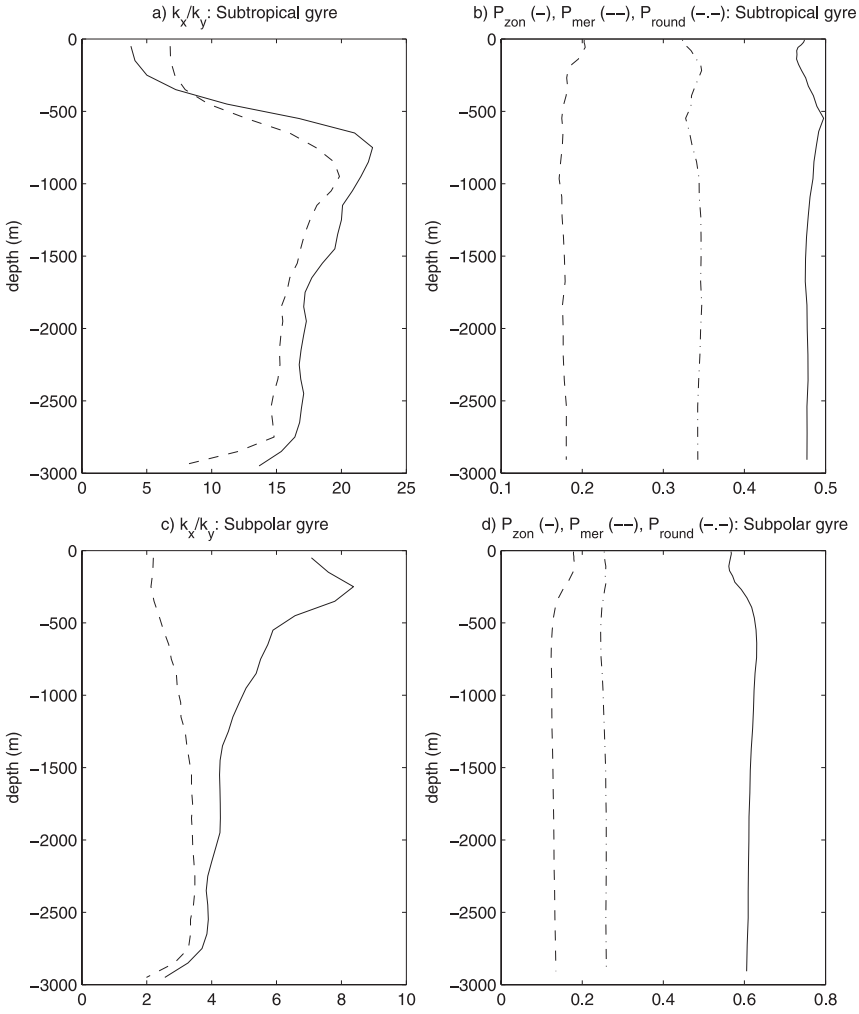

FIG. 4. Anisotropy in the spreading rates and the shape of eddies. (left) The ratio between the zonal and meridional spreading rates in the (a) subtropical and (c) subpolar regions. The solid lines show the values for the standard simulations and dashed lines for the eddy-only simulations. (right) The portion of the EKE corresponding to the zonally elongated (P_{zon}; solid lines), meridionally elongated (P_{mer}; dashed), and round eddies (P_{round}; dashed–dotted) in the (b) subtropical and (d) subpolar regions.

and between 0.56 and 0.63 in the subpolar gyres. This is consistent with the predominantly zonal material transport in this model. Round eddies have secondary importance and meridionally elongated eddies are the least important in both regions. Unlike the measure of anisotropy k_x/k_y, however, the relative importance of the zonally elongated eddies does not increase significantly with depth in the upper half of the subtropical gyre. Additionally, P_{zon} is larger in the subpolar region than in the subtropical one, whereas the k_x/k_y ratio is significantly larger in the subtropical region, particularly in the eddy-only simulations. The relative importance of the zonally elongated eddies is not, therefore, sufficient to explain changes in the anisotropy of the material transport with depth and between the subtropical and subpolar regions.

We next analyze the meridional structure of the material transports and calculate the mean spreading rates for all particles that are initially located within 0.5° of each latitude. Our approach is to assume that the mixing properties are uniform in the zonal direction—a debatable but useful assumption in this study. Figure 6 shows the resulting $k_x(y)$ and $k_y(y)$ for the upper ocean (upper 360 m). The distribution is qualitatively similar at other depths. The definition of local spreading rates is complicated by particle displacements; in the meridional direction it is approximately 1.5° on average. To account for the resulting nonlocal nature of the

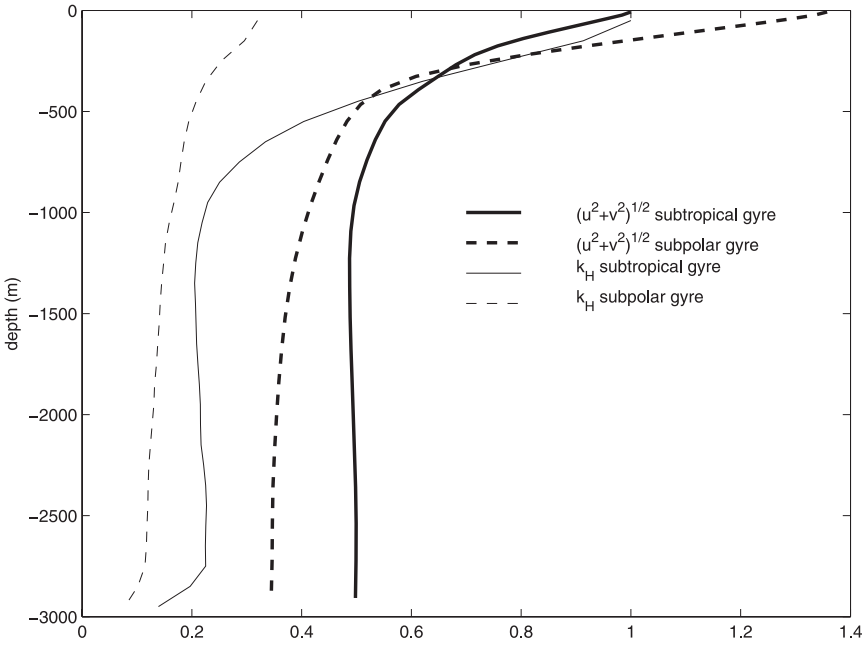

FIG. 5. Eddy velocity magnitude $(u^2 + v^2)^{1/2}$ and the mean spreading rates. Velocity magnitudes, area-averaged within the subtropical (heavy solid) and subpolar (heavy dashed) box regions (Fig. 1), are shown as functions of depth. Both functions are normalized by the mean value of the eddy velocity magnitude at the surface in the subtropical gyre. Also shown are the magnitude of the spreading rate $k_H = (k_x^2 + k_y^2)^{1/2}$ in the subtropical (thin solid) and subpolar (thin dashed) regions for the eddy-only simulation. Both functions are normalized by the value of k_H at the surface in the subtropical gyre.

computed spreading rates, we smooth the results with a 3° sliding mean filter. The corresponding values are calculated for the westernmost subgroup of particles in the subpolar gyre and for the easternmost subgroup in the subtropical gyre.

The zonal and meridional spreading rates, $k_x(y)$ and $k_y(y)$, vary with latitude in the wide ranges of 1750–12 600 and 230–2900 $m^2\ s^{-1}$, respectively, and the largest values are at 28°–30°N (Fig. 6). The location of this maximum coincides with the latitude of maximum variance in our model but is noticeably southward of a similar maximum in the observation-based estimates in Lumpkin et al. (2002), where it is located near 40°N. The overall meridional structure does not exhibit any significant correlation with the positions of the zonal jets, which can be partly due to the nonlocality of our estimates of the spreading rates. It is tempting, nevertheless, to interpret this lack of correlation as another manifestation of the modest role of the jet advection in the particle spreading. The local values of the spreading rates diagnosed from the eddy-only simulations are, however, noticeably different from those in the standard run. The largest differences are observed in the subpolar gyre (Figs. 3b,d and Fig. 6), where the zonal spreading rate $k_x(y)$ is reduced by more than 60% and the meridional spreading rate $k_y(y)$ is more than doubled. The changes are more modest in the subtropical gyre region, where the average zonal spreading is hardly changed, but the average meridional spreading rate is reduced by nearly 40%. The removal of the time-mean advection also leads to the southward shift in the $k_x(y)$ maximum. The differences in zonal spreading rates between the standard and eddy-only cases in the deep ocean are very small.

c. Asymmetry in the material transport

Here, we analyze the difference between the eastward and westward spreading and the difference between the northward and southward spreading. We introduce the following convenient measures of such asymmetry, the normalized ensemble-mean displacements:

$$a_x(y) = \frac{X(T)}{\frac{1}{N}\sum_{n=1}^{N}|x_n(T)|}, \quad a_y(y) = \frac{Y(T)}{\frac{1}{N}\sum_{n=1}^{N}|y_n(T)|}, \quad (4)$$

where $T = 180$ days. If all particle displacements are in the same direction, the functions defined by (4) will be ± 1. Alternatively, if particle displacements are purely symmetric, a_x and a_y will be zero. In the case of the equal

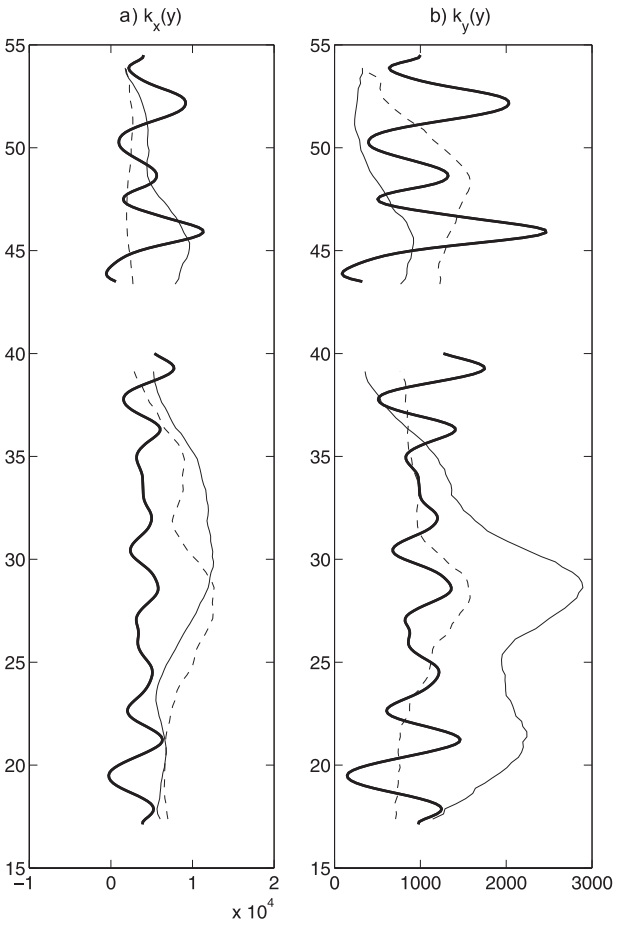

FIG. 6. (a) Zonal (k_x) and (b) meridional (k_y) spreading rates in the upper 360 m as functions of latitude. Thin solid lines show the values for the standard simulations, and dashed lines for the eddy-only simulations. Units are $m^2\ s^{-1}$. The thick lines show time-mean zonal velocities, zonally and vertically averaged. Velocity values are offset and amplified for presentation purposes.

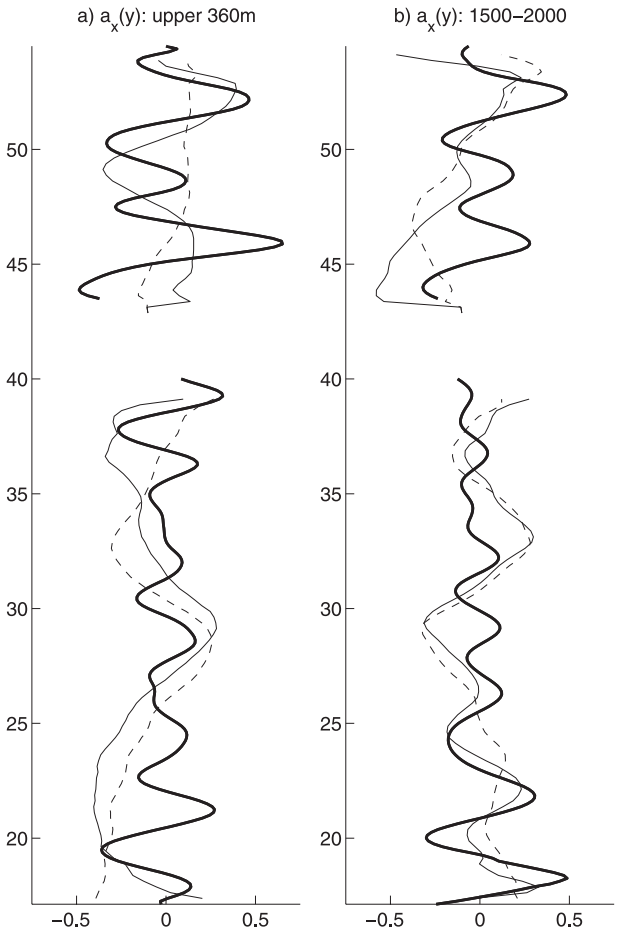

FIG. 7. Asymmetric spreading in the zonal direction. Shown by the thin lines is the measure of zonal spreading asymmetry a_x (unitless) in the (a) upper 360-m and (b) 1444–2095-m depth range. The solid lines show the standard run, and dashed lines represent an eddy-only experiment. The results are smoothed with a 3° running mean filter. The thick line shows the time-mean zonal velocities, zonally and vertically averaged. Velocity values are offset and amplified for presentation purposes.

number of particles moving in the westward and eastward directions, a_x taking the value of, for example, 0.3 implies that the average eastward displacement is 86% greater than the westward one. As in (1), the displacements in (4) are corrected for the large-scale advection.

The results demonstrate asymmetric spreading, particularly in the zonal direction (Fig. 7). The measure of zonal asymmetry a_x exceeds the value of ± 0.3 at several locations, indicating significant asymmetry in the ensemble-mean zonal particle displacements. In the upper 360 m of the subpolar gyre and in the southern part of the deep subtropical gyre, the maxima in a_x coincide with the jet axes. The removal of the time-mean advection in the eddy-only experiments results in the drastic reduction in the size of a_x, which indicates nearly symmetric particle displacements. These facts suggest that the zonal displacements of particles are ''skewed'' by the jets in these regions. The opposite situation is observed in the upper-ocean subtropical gyre and in the entire deep ocean north of 27°N. Here, the magnitude of a_x is similar between the standard and eddy-only cases and exhibits maxima that do not appear to be associated with the jets. The average magnitudes of a_x in the upper and deep ocean are 0.2 and 0.16 in the standard and 0.17 and 0.16 in the eddy-only cases. A measure of asymmetry in the meridional direction has an average magnitude of 0.22–0.2 in the upper and 0.12–0.11 in the deep ocean in the standard eddy-only cases.

To further quantify the asymmetry in the particle spreading, we calculate the skewness of the particle distribution at day 180, both in the zonal and meridional directions:

$$\gamma_x = \frac{1}{D_x^{3/2}} \frac{1}{N} \sum_{n=1}^{N} [x_n(T) - X(T)]^3,$$

$$\gamma_y = \frac{1}{D_y^{3/2}} \frac{1}{N} \sum_{n=1}^{N} [y_n(T) - Y(T)]^3. \quad (5)$$

Unlike the measure (4), the skewness in (5) describes the asymmetry in the particle distribution around the ''center of mass'' of all particles in the group. In the upper subpolar gyre, such distribution is nearly symmetric with respect to the center of mass and the magnitudes of zonal and meridional skewness vary between 0.1 and 0.16 for both standard and eddy-only cases (Table 1). In contrast, the upper subtropical gyre in the standard case exhibits an asymmetric particle distribution with the zonal and meridional skewness of 0.41 and −0.34. This asymmetry is primarily due to the time-mean advection, since in the eddy-only simulations the zonal and meridional skewness is substantially reduced. In the deep subtropical gyre, the particle distribution is significantly asymmetric in the zonal direction with a large negative skewness of −0.53 in the standard and −0.72 in the eddy-only cases. Similarly, in the deep subpolar gyre the skewness in the eddy-only case is also large and negative (−0.45). These results are consistent with the westward increase in the velocity amplitude in the deep layers (Fig. 1b). The distribution of particles in the deep ocean is nearly symmetric in the meridional direction.

TABLE 1. Zonal (γ_x) and meridional (γ_y) skewness in particle distribution at day 180.

	Subtropical (standard case)	Subtropical (eddy-only case)	Subpolar (standard case)	Subpolar (eddy-only case)
γ_x (0–360 m)	0.41	0.2	0.1	0.16
γ_y (0–360 m)	−0.34	−0.08	0.12	−0.14
γ_x (1500–2000 m)	−0.53	−0.72	0.07	−0.45
γ_y (1500–2000 m)	0	0.05	−0.13	−0.06

4. Summary and discussion

We present an analysis of the anisotropic properties of the material transport by eddies and eddy-driven time-mean currents, as estimated from the trajectories of neutrally buoyant particles in a model of the North Atlantic. The eddy-driven time-mean currents consist of the alternating zonal jets and the meridional motions associated with acceleration and deceleration of these jets. The eddies, therefore, affect tracer distribution in two major ways: 1) by advecting the tracer (direct effect) and 2) by supporting the jets (indirect effect). Neither the direct nor indirect effects can be reproduced by non-eddy-permitting simulations and thus have to be parameterized. These two effects are particularly difficult to separate from each other in observational studies and the diffusivity estimates from drifter trajectories include the effects of the alternating time-mean zonal jets. In the numerical simulations like ours, the separation of these effects is straightforward and is achieved with the use of simulations in which the time-mean velocities are removed from the particle advection.

We discuss three main anisotropic properties of the material transport: 1) the difference between the zonal and meridional directions, 2) variations with the latitude and in the vertical, and 3) asymmetry. Spreading rates, which are defined here as half the rate of change in the particle dispersion in the zonal direction, systematically exceed the meridional ones by an order of magnitude. The area-averaged values for the upper-ocean zonal and meridional spreading rates are approximately 8100 and 1400 $m^2\ s^{-1}$, respectively, and in the deep ocean they are 2400 and 200 $m^2\ s^{-1}$. The analysis of the simulations with the removed time-mean advection (''eddy-only'' simulations) demonstrates that this anisotropy is mainly due to the action of eddies and not to the shear dispersion associated with the time-mean jets. The direct effect of eddies is also the main cause of the superdiffusive zonal spreading in most of the computational domain (except the upper-ocean subpolar region), of significant variations in the spreading rates in the vertical and meridional direction, and of the asymmetry in the zonal spreading.

The modest role of the shear dispersion of the time-mean jets is in contrast to the dramatic effects of the shear dispersion in the flow with an isotropic eddy field and zonally uniform stationary jets, as analyzed in Smith (2005). We can think of three plausible explanations for the difference. First, the time-mean velocity shear in our study is two-dimensional and its overall effect on tracer spreading is, thus, more complicated than that in the classical shear dispersion problem (Taylor 1953). Second, our jets are ''latent'' and the flow is dominated by the transient eddies; the secondary importance of the shear dispersion can thus be viewed as another manifestation of the latent nature of the jets. The time-mean jets are particularly weak in the subtropical gyre, and consistent with that the effects of the shear dispersion are weak as well. Additionally, the eddy field in this study is dominated by anisotropic, zonally elongated eddies, which have a longer correlation scale in the zonal direction. Such eddies are expected to result in the predominantly zonal Lagrangian velocities (appendix) and zonal material transport. The term ''shear dispersion''

can, therefore, be equally applied to the dispersive effects of these zonally elongated eddies. These potentially important eddy effects are, however, not straightforward enough to isolate in this study.

The only region that is in a general agreement with the properties of the dispersion in the flow with one-dimensional shear, as discussed by Smith (2005), is the upper 500 m of the subpolar gyre. Here, the zonal spreading is substantially weakened and the meridional spreading is enhanced in the eddy-only simulations, as compared to the standard runs. The spreading in this region is, therefore, more isotropic in the eddy-only simulations. However, the difference between the zonal and meridional transports in the eddy-only simulations is still large (more than 100%) even in this region. The removal of the time-mean advection by the jets and their meridional currents also results in the nearly diffusive spreading of particles in the upper-ocean subpolar gyre, whereas the zonal spreading is almost always super-diffusive in the rest of the domain. These results are largely consistent with the fact that the jets are particularly strong and nearly steady in the subpolar region.

Spatial variations in the spreading rates are large everywhere. Spreading rates decrease away from the surface, in accordance with the downward decrease in the eddy variance. The spreading in the subtropical gyre becomes less isotropic with depth, whereas in the subpolar gyre it becomes more isotropic with depth. This difference between the gyres is explained by the effects of the jets, because in the eddy-only simulations both regions exhibit less isotropic spreading rates in the deep ocean than near the surface. The spreading rates also vary strongly in the meridional direction, and most significantly many properties of the material transports discussed in this study differ between the subtropical and subpolar gyres. Significant dynamical differences between these two regions were reported in KBP09 for the same model, but the reasons for the differences were not determined. They are possibly tied to the more unstable background flow and more uniform stratification in the subpolar region. The difference between the subtropical and subpolar gyres can also be explained by the more prominent topography in the latter region, since the drifters in the real ocean are shown to follow the f/H contours (LaCasce 2000).

The amplitudes and anisotropic shapes of eddies are generally consistent with some properties of the material transport but do not fully explain the dependence of the spreading rates on depth and latitude. In particular, and largely in concert with the spreading rates, the eddy velocity magnitude decreases with depth but cannot explain large differences in the spreading rates between the subtropical and subpolar gyres. The eddy field is also dominated by eddies elongated in the zonal direction, as is visible from the velocity plots and confirmed by the analysis of the spatial spectra. The relative importance of the zonally elongated eddies, however, is not sufficient to explain changes in the material transport with depth and latitude. Most notably, very strong anisotropy in the material transport in the subsurface subtropical gyre remains unexplained by the above arguments.

Our analysis results in the estimates of the average zonal and meridional spreading rates. In particular, our estimated values for K_x are significantly larger than the values for horizontal or isopycnal tracer diffusivities typically used in non-eddy-permitting models (200–1000 $m^2\ s^{-1}$). However, caution should be exercised if these values are used as guidance for the diffusivities in non-eddy-permitting models. The direct comparison between the eddy-permitting and non-eddy-permitting simulations is challenging, partly because of the very different time-mean circulations. We also find that the zonal spreading of particles in our model is super-diffusive, at least during each 180-day simulation, which is primarily due to the eddy rather than the time-mean advection. In contrast, the meridional spreading is more consistent with the diffusive model. Proximity of the solid boundaries, however, precluded us from examining the spreading regimes at significantly longer times, which are sometimes needed to approach a purely diffusive regime (Lee et al. 2009). The difference between the zonal and meridional dispersion regimes is in agreement with Berloff et al. (2002), who reported similar behavior in the western part of their double-gyre model. These nondiffusive effects cannot be captured by a diffusive model but can have potentially important implications for tracer studies. It is not clear how such effects can be parameterized in non-eddy-permitting simulations.

The material transports due to eddies and eddy-driven currents also tend to be asymmetric, particularly in the zonal direction. The normalized ensemble-averaged displacements demonstrate that several time-mean zonal jets act to set the preferred direction for the zonal material transport. This property makes it possible to detect zonal jets in the distributions of tracers that have strong zonal gradient. The transient eddies also cause significant asymmetry in spreading, particularly in the deep ocean, as demonstrated by the eddy-only simulations. This is further illustrated by the skewness in the particle distribution, which, in the zonal direction, tends to be large and negative in the deep layers of the eddy-only simulations. The westward increase in the eddy variance is the most plausible cause of negative skewness in the deep ocean. Additionally, nonuniform spatial distribution and temporal increase of zonal spreading rates can also result in spreading asymmetry.

The significance of the reported anisotropy for distribution of oceanic tracers remains to be addressed. Distribution of any tracer is a result of a complicated interplay between the time-mean advection, convection, and mixing by eddies and small-scale processes (e.g., Booth and Kamenkovich 2008). Large differences between the zonal and meridional directions, as well as nondiffusive eddy-induced transports in the zonal direction, call for further studies.

Acknowledgments. The authors thank Dr. S. Smith and an anonymous reviewer for their helpful advice on improving this manuscript. Funding for IK was provided by NSF Grants OCE 0346178, 0749722, and 0842834. Funding for PB was provided by NSF Grants OCE 0344094 and OCE 0725796 and by the research grant from the Newton Trust of the University of Cambridge. For JP the acknowledgement is to NSF OCE-0451086.

APPENDIX

Time-Mean Lagrangian Velocities in an Elongated Eddy

Consider a wavelike geostrophic disturbance with the streamfunction of the form $\psi = h(x, y)\cos(kx + ly - \omega t)$, where (k, l) are the zonal and meridional wavenumbers, ω is the frequency, and $h(x, y)$ is the amplitude function. The zonal and meridional velocities are then given, respectively:

$$u = -\frac{\partial h}{\partial y}\cos(kx + ly - \omega t) + hl\sin(kx + ly - \omega t),$$
$$v = \frac{\partial h}{\partial x}\cos(kx + ly - \omega t) - hk\sin(kx + ly - \omega t). \quad \text{(A1)}$$

The Lagrangian velocity of a fluid element is given, to the first order, by

$$u_L \approx u + (\xi_x - x)\frac{\partial u}{\partial x} + (\xi_y - y)\frac{\partial u}{\partial y},$$
$$v_L \approx v + (\xi_x - x)\frac{\partial v}{\partial x} + (\xi_y - y)\frac{\partial v}{\partial y}, \quad \text{(A2)}$$

where the particle displacements ξ_x and ξ_y can also be easily calculated from (A1):

$$\xi_x = x + \frac{1}{\omega}\frac{\partial h}{\partial y}\sin(kx + ly - \omega t) + \frac{hl}{\omega}\cos(kx + ly - \omega t),$$
$$\xi_y = y - \frac{1}{\omega}\frac{\partial h}{\partial x}\sin(kx + ly - \omega t) - \frac{hk}{\omega}\cos(kx + ly - \omega t). \quad \text{(A3)}$$

Averaging (A2) over the time period $1/\omega$ leads to the following expressions for the time-mean Lagrangian velocities $\overline{u}_L$ and $\overline{v}_L$:

$$\overline{u}_L = \frac{1}{4\omega}\left(-l\frac{\partial}{\partial x} + k\frac{\partial}{\partial y}\right)\frac{\partial}{\partial y}h^2,$$
$$\overline{v}_L = \frac{1}{4\omega}\left(l\frac{\partial}{\partial x} - k\frac{\partial}{\partial y}\right)\frac{\partial}{\partial x}h^2. \quad \text{(A4)}$$

The orientation of the time-mean Lagrangian velocity is determined, to a large extent, by the ratio between the zonal and meridional scales of the amplitude function $h(x, y)$. If the zonal scale is considerably longer than the meridional one, the Lagrangian velocity is nearly zonal. For a Rossby wave in a channel $-L < y < L$, $l = 0$, $h(x, y) = A\sin[(\pi n/L)y]$, and the time-mean Lagrangian velocity is purely zonal.

REFERENCES

Bauer, S., M. S. Swenson, and A. Griffa, 2002: Eddy mean flow decomposition and eddy diffusivity estimates in the tropical Pacific Ocean: 2. Results. *J. Geophys. Res.,* **107,** 3154, doi:10.1029/2000JC000613.

Berloff, P., J. McWilliams, and A. Bracco, 2002: Material transport in oceanic gyres. Part I: Phenomenology. *J. Phys. Oceanogr.,* **32,** 764–796.

——, I. Kamenkovich, and J. Pedlosky, 2009: A model of multiple zonal jets in the oceans: Dynamical and kinematical analysis. *J. Phys. Oceanogr.,* **39,** 2711–2734.

Booth, J., and I. Kamenkovich, 2008: Isolating the role of transient mesoscale eddies in mixing of a passive tracer in an eddy resolving model. *J. Geophys. Res.,* **113,** C05021, doi:10.1029/2007JC004510.

Boyer, T., S. Levitus, H. Garcia, R. Locarnini, C. Stephens, and J. Antonov, 2005: Objective analyses of annual, seasonal, and monthly temperature and salinity for the World Ocean on a 0.25 degree grid. *Int. J. Climatol.,* **25,** 931–945.

Cessi, P., and M. Fantini, 2004: The eddy-driven thermocline. *J. Phys. Oceanogr.,* **34,** 2642–2658.

Davis, R. E., 1991: Observing the general circulation with floats. *Deep-Sea Res.,* **38** (Suppl. 1), 531–571.

Galperin, B., H. Nakano, H. Huang, and S. Sukoriansky, 2004: The ubiquitous zonal jets in the atmospheres of giant planets and Earth's oceans. *Geophys. Res. Lett.,* **31,** L13303, doi:10.1029/2004GL019691.

Gille, S., and R. Davis, 1999: The influence of mesoscale eddies on coarsely resolved density: An examination of subgrid-scale parameterization. *J. Phys. Oceanogr.,* **29,** 1109–1123.

Henning, C. C., and G. Vallis, 2005: The effects of mesoscale eddies on the stratification and transport of an ocean with a circumpolar channel. *J. Phys. Oceanogr.,* **35,** 880–896.

Hogg, N., and B. Owens, 1999: Direct measurement of the deep circulation within the Brazil basin. *Deep-Sea Res.,* **46,** 335–353.

Huang, H.-P., A. Kaplan, E. Curchitser, and N. Maximenko, 2007: The degree of anisotropy for mid-ocean currents from satellite observations and an eddy-permitting model simulation. *J. Geophys. Res.,* **112,** C09005, doi:10.1029/2007JC004105.

Kamenkovich, I., P. Berloff, and J. Pedlosky, 2009: Role of eddy forcing in the dynamics of multiple zonal jets in the North Atlantic. *J. Phys. Oceanogr.,* **39,** 1361–1379.

LaCasce, J. H., 2000: Floats and f/h. *J. Mar. Res.,* **58,** 61–85.

——, 2008: Statistics from Lagrangian observations. *Prog. Oceanogr.,* **77,** 1–29.

——, and A. Bower, 2000: Relative dispersion in the subsurface North Atlantic. *J. Mar. Res.,* **58,** 863–894.

Ledwell, J. R., A. J. Watson, and C. S. Law, 1993: Evidence for slow mixing across the pycnocline from an open-ocean tracer-release experiment. *Nature,* **364,** 701–703.

Lee, M.-M., A. J. G. Nurser, A. C. Coward, and B. A. de Cuevas, 2009: Effective eddy diffusivities inferred from a point release tracer in an eddy-resolving ocean model. *J. Phys. Oceanogr.,* **39,** 894–914.

Lumpkin, R., A.-M. Treguier, and K. Speer, 2002: Lagrangian eddy scales in the northern Atlantic Ocean. *J. Phys. Oceanogr.,* **32,** 2425–2440.

Marshall, J., E. Shuckburgh, H. Jones, and C. Hill, 2006: Estimates and implications of surface eddy diffusivity in the Southern Ocean derived from tracer transport. *J. Phys. Oceanogr.,* **36,** 1806–1821.

Maximenko, N., B. Bang, and H. Sasaki, 2005: Observational evidence of alternating zonal jets in the world ocean. *Geophys. Res. Lett.,* **32,** L12607, doi:10.1029/2005GL022728.

Nakamura, M., and Y. Chao, 2000: On the eddy isopycnal thickness diffusivity of the Gent–McWilliams subgrid mixing parameterization. *J. Climate,* **13,** 502–510.

Nakano, H., and H. Hasumi, 2005: A series of zonal jets embedded in the broad zonal flows in the Pacific obtained in eddy-permitting ocean general circulation models. *J. Phys. Oceanogr.,* **35,** 474–488.

Owens, W. B., 1984: A synoptic and statistical description of the Gulf Stream and subtropical gyre using SOFAR floats. *J. Phys. Oceanogr.,* **14,** 104–113.

Pacanowski, R. C., and S. M. Griffies, 1999: MOM 3.0 manual. NOAA/GFDL Tech. Rep., 680 pp.

Radko, T., and J. Marshall, 2004: Eddy-induced diapycnal fluxes and their role in the maintenance of the thermocline. *J. Phys. Oceanogr.,* **34,** 372–383.

Rhines, P., 1994: Jets. *Chaos,* **4,** 313–339.

Richards, K., N. Maximenko, F. Bryan, and H. Sasaki, 2006: Zonal jets in the Pacific Ocean. *Geophys. Res. Lett.,* **33,** L03605, doi:10.1029/2005GL024645.

Roberts, M., and D. Marshall, 2000: On the validity of downgradient eddy closures in ocean models. *J. Geophys. Res.,* **105,** 28 613–28 627.

Sallee, J.-B., K. Speer, R. Morrow, and R. Lumpkin, 2008: An estimate of Lagrangian eddy statistics and diffusion in the mixed layer of the Southern Ocean. *J. Mar. Res.,* **66,** 441–463.

Scott, R. B., B. K. Arbic, C. L. Holland, B. Qiu, and A. Sen, 2008: Zonal versus meridional velocity variance in satellite observations and realistic and idealized ocean circulation models. *Ocean Modell.,* **23,** 102–112.

Smith, K. S., 2005: Tracer transport along and across coherent jets in two-dimensional turbulent flow. *J. Fluid Mech.,* **544,** 133–142.

Talley, L. D., 2003: Shallow, intermediate, and deep overturning components of the global heat budget. *J. Phys. Oceanogr.,* **33,** 530–560.

Taylor, G. I., 1953: Dispersion of soluble matter in solvent flowing slowly through a tube. *Proc. Roy. Soc. London,* **A219,** 186–203.

Thompson, A., and W. Young, 2007: Baroclinic eddy heat fluxes: zonal flows and energy balance. *J. Atmos. Sci.,* **64,** 3214–3231.

Treguier, A., N. Hogg, M. Maltrud, K. Speer, and V. Thierry, 2003: The origin of deep zonal flows in the Brazil basin. *J. Phys. Oceanogr.,* **33,** 580–599.

Veneziani, M., A. Griffa, A. M. Reynolds, Z. D. Garraffo, and E. P. Chassignet, 2005: Parameterizations of Lagrangian spin statistics and particle dispersion in the presence of coherent vortices. *J. Mar. Res.,* **63,** 1057–1083.

Young, W. R., P. B. Rhines, and C. J. R. Garrett, 1982: Shear-flow dispersion, internal waves and horizontal mixing in the oceans. *J. Phys. Oceanogr.,* **12,** 515–527.